Surveys in Geophysics
https://doi.org/10.1007/s10712-024-09850-y

Q: A Review

José M. Carcione[1,2] · Francesco Mainardi[3] · Ayman N. Qadrouh[4] · Mamdoh Alajmi[4] · Jing Ba[1]

Received: 5 March 2024 / Accepted: 26 June 2024

Abstract
The quality factor Q is a dimensionless measure of the energy loss per cycle of a wave field, and a proper understanding of this factor is important in a variety of fields, from seismology, geophysical prospecting to electrical science. Here, the focus is on viscoelasticity. When interpreting experimental values, several factors must be taken into account, in particular the shape of the medium (rods, bars or unbounded media) and the fact that the measurements are made on stationary or propagating modes. From a theoretical point of view, the expressions of Q may differ due to different definitions, the spatial dimension and the inhomogeneity of the wave, i.e. the fact that the vectors of propagation (or wavenumber) and attenuation do not point in the same direction. We show the difference between temporal and spatial Q, the relationships between compressional and shear Q, the dependence on frequency, the case of poro-viscoelasticity and anisotropy, the effect of inhomogeneous waves and various loss mechanisms, and consider the analogy between elastic and electromagnetic waves. We discuss physical theories describing relaxation peaks, bounds on Q and experiments showing the behaviour of Q as a function of frequency, saturation and pore pressure. Finally, we propose an application example where Q can be used to estimate porosity and saturation.

Keywords Quality factor · Definitions · Temporal Q · Spatial Q · Inhomogeneous waves · Electrical analogies · Anisotropy · Poro-viscoelasticity

✉ Jing Ba
jingba@188.com

[1] National Institute of Oceanography and Applied Geophysics - OGS, 34010 Sgonico TS, Italy

[2] School of Earth Sciences and Engineering, Hohai University, 211100 Nanjing, China

[3] Department of Physics and Astronomy, University of Bologna, Bologna, Italy

[4] KACST, PO Box 6086, 11442 Riyadh, Saudi Arabia

Published online: 26 July 2024

Article Highlights

- We review the concept of quality factor, including experimental and theoretical research published during the last 60 years
- We point out many cases that lead authors to misinterpret Q depending on many factors such different definitions, dimensionality of the medium, type of wave and the case of porous media
- We consider the effects of anisotropy and thermo-elasticity, bounds in the case of composite media, and the analogy with electromagnetism
- Finally, we propose an application, where Q can be used to estimate porosity and saturation

1 Introduction

The term Q was first introduced in 1914 to describe the ratio of reactance to effective resistance of a coil and later extended to mechanical and acoustic resonators as well as quantum systems such as spectral lines and particle resonances (Green 1955). A related concept is the logarithmic decrement π/Q, defined as $\ln(\max_0/\max_1)$, the natural logarithm of the ratio of two consecutive maxima in a damped wave train (Green 1955). Another form is the loss tangent, which corresponds to the dissipation factor $1/Q$.

An overview for geophysics was published in Knopoff (1964) (see also Qadrouh et al. 2024). Seismic attenuation has a decisive influence on the signal and is therefore important for the synthesis of the waveform. It is parameterized by the quality factor Q, which accounts for the total energy loss of the seismic pulse during propagation and is a key parameter for extracting information about the subsurface layers, such as porosity, permeability, fluid saturation and viscosity (Carcione 2022; Gurevich and Carcione 2022). In electrical science, the quality factor Q of a circuit is important in electromagnetic waveguides and radio-frequency cavities. It measures the “goodness" or quality of a resonant circuit. A higher value corresponds to a narrow bandwidth, which is desirable in many applications (Green 1955).

The expressions for Q used for the evaluation of experiments can be different. The distinction between spatial and temporal quality factors, Q and Q_T, is important in seismology, for example, where the anelastic properties of free earth oscillations (or normal modes) are strictly different from those of teleseismic waves. In Knopoff et al. (1964), a relationship between these two different quality factors was proposed, based on an expression that involves the group velocity and applies to low-loss media, i.e. media where the quality factor is much greater than 1. (In practice, a value greater than 10 is usually common.) In the same way, ultrasonic and resonant rod measurements for estimating wave attenuation in the laboratory (see Carcione 2022), appendices B1 and B2, respectively) give different values. In the first case, a wave travels through the sample in only one direction at a time; interference effects do not occur. In the second case, a sample is made to oscillate in one of its eigenmodes so that a standing wave is formed.

The analysis of standing and propagating waves presented here is based on a theoretical analysis based on an energy balance in one-dimensional space, which is given in Carcione (2022, Section 2.3). If ω_I and α are the temporal and spatial attenuation factors, $\exp(-\omega_I t)$ and $\exp(-\alpha x)$ are the standing and propagating decays, respectively, where t and x are the temporal and spatial variables, respectively. The analysis is usually based on mechanical models of viscoelasticity, such as the Maxwell, Kelvin–Voigt, Zener and Burgers models (Carcione 2022, Section 2) (Gurevich and Carcione 2022, Section 1) in order of complexity, but this does not imply a loss of generality.

2 Complex Modulus and Fourier Wave Kernel

Let us introduce, for simplicity, the frequency-domain viscoacoustic stress–strain relation in 3D space,

$$\sigma = M\epsilon, \tag{1}$$

(see Carcione 2022, Section 3), where σ is the trace of the stress tensor, $M(\omega)$ is a complex and frequency-dependent bulk modulus, obtained as the Fourier transform of the time derivative of the relaxation function (see Carcione 2022, Eq. 2.31), ϵ is the trace of the strain tensor ($\epsilon = \partial_i u_i$), where u_i are the displacements, and $\omega = 2\pi f$ is the angular frequency, with f the frequency in Hz. The Einstein implicit summation is assumed. In the context of wave propagation, Eq. (1) is combined with the equations of momentum conservation to obtain the wave equation (Carcione 2022). Equation (1) corresponds to compressional or sound waves. Alternatively M can be a shear modulus μ for pure SH waves (see Carcione 2022, Section 4.6).

It is important the concept of wave inhomogeneity (see Carcione 2022, Section 3.3.1). In general, we consider propagating waves whose kernel in the frequency-wavenumber domain (or Fourier component) is

$$\exp[\mathrm{i}(\omega t - \mathbf{k}\cdot\mathbf{x})], \tag{2}$$

where $\mathbf{x}$ is the position vector,

$$\mathbf{k} = \boldsymbol{\kappa} - \mathrm{i}\boldsymbol{\alpha} \tag{3}$$

where $\boldsymbol{\kappa}$ is the real wavevector, $\boldsymbol{\alpha}$ is the attenuation vector and $\mathrm{i} = \sqrt{-1}$. When these vectors coincide in direction, the plane wave is called homogeneous; when these vectors differ in their direction (making an inhomogeneity angle γ), the plane wave is called inhomogeneous. In the following, we distinguish between propagating and standing waves.

Complex and frequency-dependent stiffness or moduli imply velocity dispersion and wave attenuation, the former being the increase of wave velocity with frequency, a phenomenon generally related to the strain or potential energy being complex (Carcione 2022).

3 Spatial and Temporal *Q*

For the following equations, we refer to Carcione (2022), Section 2.3). The Fourier component of a propagating wave is

$$\exp[\mathrm{i}(\omega t - k_i x_i)], \qquad k = \sqrt{\sum_i k_i^2} = \kappa - \mathrm{i}\alpha, \tag{4}$$

where k_i are the complex wavenumber components, and κ is the real wavenumber, which can be different from that of a standing wave. The complex velocity is

$$v_c = \frac{\omega}{k} = \sqrt{\frac{M}{\rho}}, \tag{5}$$

and the phase velocity and attenuation factor are

$$v_p = \frac{\omega}{\kappa} = \left[\mathrm{Re}\left(\frac{1}{v_c}\right)\right]^{-1} \quad \text{and} \qquad \alpha = -\omega \mathrm{Im}\left(\frac{1}{v_c}\right), \tag{6}$$

, respectively.

For a standing wave, we have

$$\exp[\mathrm{i}(\Omega t - \kappa_i x_i)], \qquad \Omega = \omega + \mathrm{i}\omega_I, \tag{7}$$

where Ω is the complex frequency, and the wavenumber components κ_i are real. The wavenumber is $\kappa = \sqrt{\sum_i \kappa_i^2}$.

In this case, the complex velocity is

$$v_c = \frac{\Omega}{\kappa} = \sqrt{\frac{M}{\rho}} \tag{8}$$

and the phase velocity and attenuation factor are

$$v_p = \frac{\mathrm{Re}(\Omega)}{\kappa} = \mathrm{Re}(v_c) \quad \text{and} \quad \omega_I = \kappa\, \mathrm{Im}\big(v_c\big) = \frac{\omega}{v_p} \cdot \mathrm{Im}\big(v_c\big), \tag{9}$$

, respectively.

For both modes (propagating and standing), the spatial and temporal quality factors (Q and Q_T, respectively) have the following form

$$\frac{\mathrm{Re}(M)}{\mathrm{Im}(M)} = \frac{\mathrm{Re}(v_c^2)}{\mathrm{Im}(v_c^2)} = \frac{\mathrm{Re}(\Omega^2)}{\mathrm{Im}(\Omega^2)} = -\frac{\mathrm{Re}(k^2)}{\mathrm{Im}(k^2)} \tag{10}$$

($\omega \geq 0$ and convention $\exp(+\mathrm{i}\omega t)$), but they differ, because the complex velocities differ. For example, it can be shown that for a Kelvin–Voigt mechanical model, the relation is $Q_T = \sqrt{Q^2 - 1}$ (Carcione and Ba 2024).

3.1 Knopoff et al. Relations

Knopoff et al. (1964) showed that the temporal and spatial quality factors are related as $Q_T = (v_p/v_g)Q$, where $v_g = \partial\omega/\partial\kappa$ and $v_p = \omega/\kappa$ are the spatial group and phase velocities, respectively. Moreover, they showed that $\omega_I = v_g\alpha$. In their calculations, they assumed low-loss media, isotropy and 1D propagation. They conclude that the Q_T's measured from observations of the Earth's free vibration modes must be modified when compared to the Q's at the same periods obtained from experiments with propagating waves. The simplest case is the dispersionless model used by Carcione et al. (2016) to perform seismic migration in the presence of attenuation. Indeed, in the absence of dispersion there is no distortion of the wave packet and the group and phase velocities are the same, which means that the temporal and spatial quality factors coincide. For instance, the pressure wave equation is $\ddot{p} = c^2\partial_{xx}p - 2\gamma\dot{p} - \gamma^2 p$, where p is the pressure, c is a velocity, γ is a damping parameter and an overdot denotes time differentiation. It is easy to show that $v_c = c/(1 - \mathrm{i}\gamma/\omega)$, $v_{cT} = c(1 + \mathrm{i}\gamma/\omega)$, $v_p = v_g = c$, $\omega_I = \gamma$, $\kappa = \kappa_T = \omega/c$ and $Q_T = Q = (\omega^2 - \gamma^2)/(2\gamma\omega)$.

4 Other Definitions of Q

The quality factor

$$Q = \frac{\mathrm{Re}(v_c^2)}{\mathrm{Im}(v_c^2)} \tag{11}$$

is the elastic energy stored in a medium divided by the energy dissipated in one period of the wave field. The stored energy is usually assumed to be twice the potential (strain) energy or alternatively the total energy ($\mathcal{Q}$ according to Buchen 1971, for which the expressions for low-loss media are equal ($Q \gg 1$) (Carcione 2022, Section 2.3.1). In general, and for homogeneous waves,

$$\mathcal{Q} = \frac{[\mathrm{Re}(v_c)]^2}{\mathrm{Im}(v_c^2)} \tag{12}$$

(Carcione 2022, Eq. 3.131). The relation between the quality factors is

$$\mathcal{Q} = \frac{1}{2}\left(\sqrt{1+Q^2}+Q\right) \tag{13}$$

(Carcione 2022, Eq. 2.128). The exact equations for the attenuation factors α are

$$\frac{2\pi f}{v_p}\left(\sqrt{1+Q^2}-Q\right) \quad \text{and} \quad \frac{\pi f}{\mathcal{Q} v_p}, \tag{14}$$

which, despite the different expressions, are approximately the same regardless the value of Q.

The quality factor can also be defined as the peak or maximum potential energy divided by the dissipated energy (Borcherdt 2009, Eqs. 1.2.8 and 1.2.9; Mainardi 2022, Eq. 2.62). This definition is equivalent to Eq. (11), defined with the average strain energy when all the strain components are in phase (Carcione and Cavallini 1993 Eq. A.7; Carcione 2022, Eq. 4.76), i.e. when the peak strain energy is twice the average strain energy.

In addition, an instantaneous quality factor (IQ) can be defined (Carcione 2022, Section 2.12). Signals have time-varying frequencies, which are usually interpreted using spectrograms, wavelet transforms and the concept of instantaneous frequency (IF). This is the time derivative of the phase of the complex trace, which is a complex continuation of the real trace, where the imaginary part is the Hilbert transform of the real signal. The complex curve in exponential form basically separates the amplitude (envelope) from the phase. On the other hand, the IQ quantifies the dispersion. For instance, a Ricker wavelet propagating in a homogeneous lossy medium has a singularity at the peak of the envelope. The IQ shows a shift of this singularity, compared to the lossless case, which is related to the velocity dispersion, i.e. the variation of velocity with frequency.

5 *Q* Associated to Waves and Deformations

In generally Q is associated with wave modes, such as the P, S, extensional (axial), torsional and flexural waves (Carcione 2022; Carcione and Poletto 2000). The quality factor can also be related to deformations. The most general stress–strain relation in anisotropic–viscoelastic media is

$$\boldsymbol{\sigma} = \mathbf{P} \cdot \mathbf{e}, \quad (\sigma_I = p_{IJ} e_J), \tag{15}$$

where $\boldsymbol{\sigma}$ and $\mathbf{e}$ are stress and strain arrays, and $\mathbf{P}(\mathbf{x}, \omega)$ is a 6×6 complex frequency-dependent stiffness tensor (Carcione 2022, Eq. 4.4). Each eigenvector (called eigenstrain) of the stiffness tensor defines a fundamental deformation state of the medium. We may write

$$\mathbf{P} = \sum_{I=1}^{6} \Lambda_I \, \mathbf{e}_I \otimes \mathbf{e}_I, \tag{16}$$

(, Eq. 4.13), where Λ_I and $\mathbf{e}_I$ are the eigenvalues and normalized eigenvectors of $\mathbf{P}$, respectively. The six eigenvalues—called eigenstiffnesses—represent the genuine viscoelastic constants.

In the isotropic case, the eigenvalues are $3\lambda + 2\mu$ and 2μ with multiplicity 5, where λ and μ are the Lamé constants (Carcione and Cavallini 1994). The first eigenvalue is three times the compressibility $K = \lambda + (2/3)\mu$ (or bulk modulus). A quality factor can be defined for each eigenvalue,

$$Q_I = \frac{\mathrm{Re}(\Lambda_I)}{\mathrm{Im}(\Lambda_I)}, \quad I = 1, \ldots, 6. \tag{17}$$

Wave modes are characterized by their proper complex effective stiffnesses. For instance, P, S and extensional waves by $\lambda + 2\mu$, μ and $\mu(3\lambda + 2\mu)/(\lambda + \mu)$, i.e. the P-wave, shear and Young moduli (Mavko et al. 2020, Table 2.1.1, p. 39), respectively, and similarly to Eq. (17) we may define Q_P, Q_S and Q_E. All these quality factors are related. Approximately (low-loss media),

$$\gamma^2 \left(\frac{1}{Q_P} - \frac{1}{Q_K} \right) = 2(1 - 1/n) \left(\frac{1}{Q_S} - \frac{1}{Q_K} \right) \tag{18}$$

(Gurevich and Carcione 2022, Eq. 1.2.37), where Q_K is the compressibility quality factor related to $K = \lambda + 2\mu/3$, γ is the P to S velocity ratio at some finite frequency and n is the space dimension. For $n = 1$ there is no shear wave and $Q_P = Q_K$. Similarly,

$$\frac{(1 - \nu)(1 - 2\nu)}{Q_P} = \frac{1 + \nu}{Q_E} - \frac{2(2 - \nu)}{Q_S} \tag{19}$$

and

$$\frac{3}{Q_E} = \frac{1 - 2\nu}{Q_K} + \frac{2(1 + \nu)}{Q_S} \tag{20}$$

(Mavko et al. 2020, Eq. 3.8.19), where ν is a reference Poisson ratio (Mavko et al. 2020, Table 2.1.1).

The quality factor associated with dilatational deformations, which is related to K and involved in the stress–strain relationship, is physical in nature. The relationships (18–20) do not apply to the poroelastic (Biot) case, where the damping mechanism is essentially kinetic in nature and related to the differential motion between the grains and the viscous saturating fluid. In the absence of viscosity, there is no wave loss (Gurevich and Carcione 2022, Section 2.3). Figure 1 shows the dissipation factors corresponding to the different wave modes and bulk dilatation K, where v_c are complex and frequency-dependent Biot velocities (Carcione 2022, Section 7.9), so that

$$K = \rho\left[v_c^2(\mathrm{P}) - \frac{4}{3}v_c^2(\mathrm{S})\right]$$

and

$$Y = \rho v_c^2(\mathrm{S})\left[\frac{3v_c^2(\mathrm{P}) - 4v_c^2(\mathrm{S})}{v_c^2(\mathrm{P}) - v_c^2(\mathrm{S})}\right]$$

As can be seen the compressibility attenuation has no physical meaning when the expression $Q_K = K_R/K_I$ is used, where R and I denote the real and imaginary parts. This is because this expression for Q is defined from the strain energy in the energy balance (Carcione and Cavallini 1993).

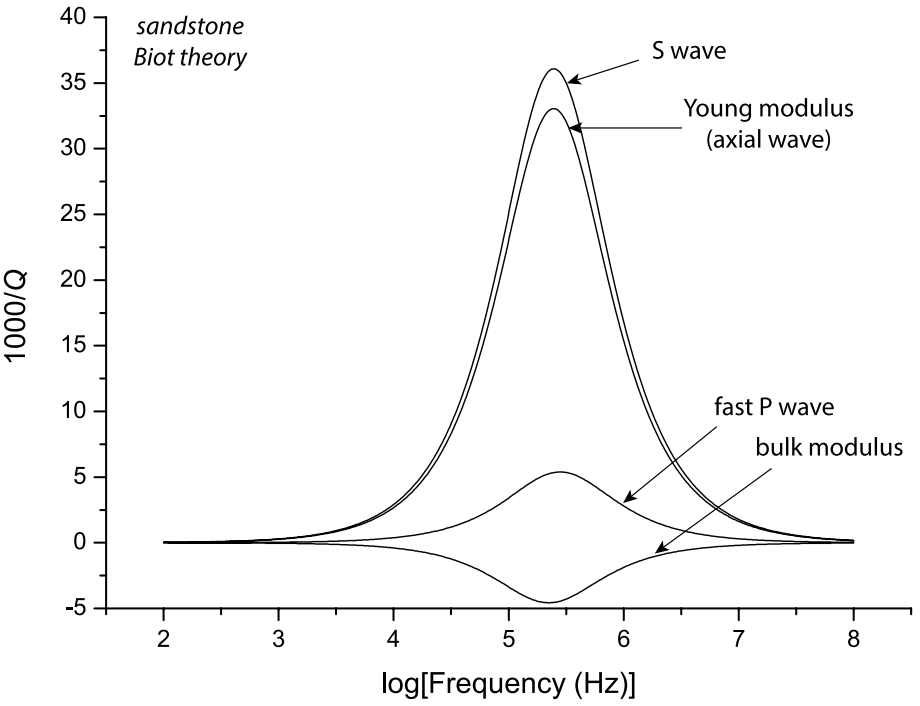

Fig. 1 Dissipation factors corresponding to different wave modes and bulk modulus K

6 Effect of the Wave Inhomogeneity

Carcione et al. (2020) compare two seemingly dissimilar expressions for the quality factor of inhomogeneous plane waves in viscoelastic media, where Q is defined as twice the strain energy to the dissipated energy. The two expressions are given in Eqs. 3.125 and 4.198 in Carcione (2022), i.e.

$$Q = \frac{\rho\omega^2 \mathrm{Re}(k^2) + 2\mu_R[\mathrm{Im}(k^2)\tan\gamma]^2}{\mathrm{Im}(k^2)[-\rho\omega^2 + 2\mu_I \mathrm{Im}(k^2)\tan^2\gamma]}. \tag{21}$$

and

$$Q = -\frac{\mathrm{Re}[(\beta^* X + \xi^* W)s_1^* + (\beta^* W + \xi^* Z)s_3^*)]}{2[\mathrm{Re}(\beta^* X + \xi^* W)\mathrm{Im}(s_1) + \mathrm{Re}(\beta^* W + \xi^* Z)\mathrm{Im}(s_3)]}. \tag{22}$$

, respectively, where the different quantities are defined in Carcione (2022, Sections 3.4.1 and 4.7.4). Those expressions which correspond to the isotropic and anisotropic cases, respectively, with the second equation being associated with the wave loss in symmetry planes of orthorhombic media. The first expression is obtained from strain and dissipation energies of Buchen (1971) (B), and the second expression uses the equations developed by Carcione and Cavallini (1993) (CV). Both expressions result in the same Q for P-waves, and Q for S-waves is independent of the inhomogeneity angle γ (in isotropic media).

Figure 2 shows the quality factors, where the solid black line corresponds to Eq. 3.125 (B) and the solid points to Eq. 4.198 (CV) of Carcione (2022). As can be seen, the two approaches are equivalent, with the P-wave Q factor decreasing with γ and the S-wave Q factors being independent of this angle. It can be shown that the S-wave quality factor for inhomogeneous waves in the isotropic poro-viscoelastic case is also independent of the inhomogeneity angle.

Furthermore, Carcione et al. (2020) provide a specific example of the anisotropic case by showing the quality factor of qP and qS waves near forbidden directions where anomalous behaviour occurs at certain propagation angles. The forbidden directions occur when the phase velocity approaches a zero value. In general, the phase velocity of homogeneous waves ($\gamma = 0$) exceeds that of inhomogeneous waves, while the latter exhibit greater attenuation (lower quality factor). Near the forbidden directions, the opposite behaviour can occur.

Explicit expressions of the quality factors (Q) for inhomogeneous waves are given in (Borcherdt 2009, Eqs. 3.4.67, 3.4.68 and 3.4.69) for P, SI, SII waves propagating in an isotropic medium, Eq. 3.125 in Carcione (2022) for P-waves, and Eq. 3.1.30 in the same book using the definition of Buchen (1971) based on the total energy ($\mathcal{Q}$) (see next section).

7 Effect of Anisotropy and Visco-Poroelasticity

Equation 7.696 in Carcione (2022), i.e.

$$Q = \frac{\mathrm{Re}(v_c^2 \underline{\boldsymbol{y}}^\top \cdot \mathbf{R} \cdot \underline{\boldsymbol{y}}^*)}{2\,\mathrm{Im}(v_c)\mathrm{Re}(v_c \underline{\boldsymbol{y}}^\top \cdot \mathbf{R} \cdot \underline{\boldsymbol{y}}^*)}, \tag{23}$$

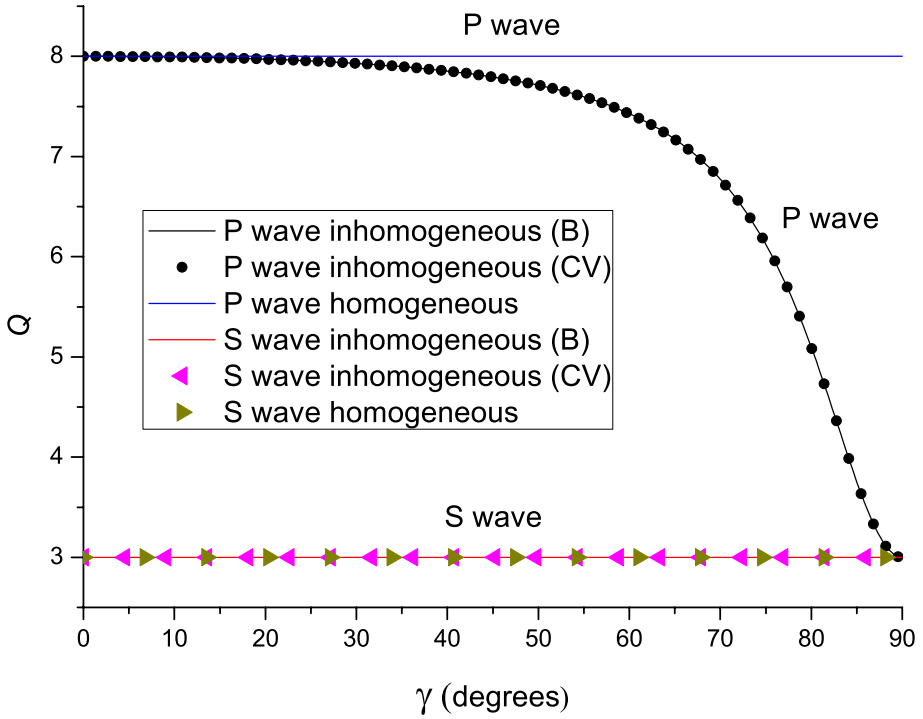

Fig. 2 Quality factor as a function of the inhomogeneity angle, based on the Buchen (1971) (B) and Carcione and Cavallini (1993) (CV) energy balances. A distinction between homogeneous and inhomogeneous waves is made

(see Section 7.24.5 for more details) gives the general quality factor for qP and qS homogeneous waves in the anisotropic poro-viscoelastic case defined in terms of the strain energy, and the corresponding energy balance is given in Carcione (2001). Only if the viscosity is zero (in the absence of Biot loss), the quality factor has the form (11), as expected, since the Biot loss is related to the kinetic energy.

On the other hand, the Buchen definition, using the total energy, of the quality factor for homogeneous waves, applied to poro-viscoelastic media, simplifies to

$$\mathcal{Q} = \frac{\mathrm{Re}(v_c)}{2\,\mathrm{Im}(v_c)} = \frac{[\mathrm{Re}(v_c)]^2}{\mathrm{Im}(v_c^2)}, \tag{24}$$

which agrees with Eq. (12).

8 Relaxation Peaks of Q^{-1} from Predictive Models and Constant Q

The Zener phenomenological model predicts a symmetric relaxation peak as a function of the logarithm of frequency. Physical or predictive models show similar relaxation peaks (Spencer 1981). Scattering loss occurs as reflection, refraction and diffraction of elastic energy, and this is conserved. A major cause of attenuation in porous media, at the

reservoir scale, is wave-induced fluid flow, which occurs at different spatial scales. The flow can be classified as macroscopic, microscopic and mesoscopic. At larger scales, grain boundary relaxation is the predominant cause of seismic attenuation in the Earth's crust and mantle. Furthermore, thermo-poroelasticity is another cause of attenuation.

8.1 Scattering

At low frequencies, when the wavelength is much larger than the characteristic scales of heterogeneity, the medium behaves like an equivalent medium, e.g. finely layered media is a transversely isotropic homogeneous medium (Backus averaging is its mathematical model) (Carcione 2022, Section 1.5). At high frequencies, scattering attenuation causes energy to be distributed into coda waves and the primary pulse behaves viscoelastically of the Zener type (Kikuchi 1981). Intrinsic (α_i) and scattering (α_s) attenuations are approximately additive, since the decay factor is $\exp(-\alpha_i x)\exp(-\alpha_s x) = \exp[-(\alpha_i + \alpha_s)x]$, and in the low-loss case ($Q \gg 1$), the total dissipation factor is

$$Q^{-1} = Q_i^{-1} + Q_s^{-1}, \tag{25}$$

based on Eq. (14). Both types of attenuation can, in principle, be separated on the basis of Eq. (25) and a proper scattering theory (Frankel and Wennerberg 1987). The location of the scattering peak is inversely proportional to the size of the heterogeneity. For instance, for cracks of length a the peak P-wave loss frequency is

$$f_s \approx \frac{v_P}{5a}, \tag{26}$$

where v_P is the P-wave velocity (Kikuchi 1981).

8.2 Wave-Induced Fluid-Flow Attenuation

Macroscopic Biot attenuation: The attenuation mechanism predicted by Biot in 1956 has a macroscopic nature (Carcione 2022, Chapter 7). It is the wavelength-scale equilibration between the peaks and troughs of the P-wave. The dissipation factor of the fast P-wave, Q^{-1}, can be approximated by that of a Zener model. The location of the relaxation peak is

$$f_B \approx \frac{\phi\eta\rho}{2\pi\bar{\kappa}\rho_f(\rho\mathcal{T} - \phi\rho_f)}, \tag{27}$$

where ϕ is the porosity, η is the fluid viscosity, ρ is the bulk density, $\bar{\kappa}$ is the permeability, ρ_f is the fluid density and $\mathcal{T}$ is the rock tortuosity. This equation shows that the relaxation peak shifts towards the high frequencies with increasing viscosity and decreasing permeability. This means that, at low frequencies, attenuation decreases with increasing viscosity (or decreasing permeability). This is inconsistent with experimental data at seismic and sonic frequencies, as the macroscopic-flow mechanism underestimates the wave velocity dispersion and attenuation in rocks.

Microscopic squirt-flow attenuation: An important attenuation mechanism in rocks is the so-called "squirt flow", in which there is a flow from fluid-filled microcracks (or grain contacts) into the pore space and back (Carcione 2022, Section 7.15). The squirt-flow model assumes that the rock becomes stiffer if the fluid pressure does not have enough time to establish equilibrium between the stiff and compliant pores (grain contacts or

main voids). This condition is described by the unrelaxed limit of the Zener elements. The squirt-flow peak frequency is

$$f_{sf} \approx \frac{K_s r^2}{3\pi\eta\gamma}, \quad \gamma = \frac{K_s}{\phi_c}\left(\frac{1}{K_m} - \frac{1}{K_h}\right), \tag{28}$$

where r is the crack thickness to crack length ratio, ϕ_c is the compliant porosity and K_s, K_m and K_h are the bulk moduli corresponding to the grain, dry rock and dry rock at a confining pressure when all compliant pores (or cracks and grain contacts) are closed, i.e. a hypothetical rock without the soft porosity, respectively.

Mesoscopic attenuation: Local fluid flow explains the high attenuation of low-frequency waves in fluid-saturated rocks. When seismic waves propagate through small-scale heterogeneities, pressure gradients are induced between regions of different properties. White (1975) was the first to show that attenuation and velocity dispersion measurements can be explained by the combined effect of mesoscopic-scale inhomogeneities and energy transfer between wave modes, with P-wave to slow P (Biot)-wave conversion being the main physical mechanism. We refer to this mechanism as mesoscopic loss. The mesoscopic-scale length is intended to be larger than the grain sizes but much smaller than the wavelength of the pulse. A review of the different theories and authors, who have contributed to the understanding of this mechanism, can be found in Müller et al. (2010) (see also Carcione 2022, Section 7.16; Gurevich and Carcione 2022). At seismic frequencies, the mesoscopic loss mechanism seems to be dominant. Mesoscopic patches of gas in a water-saturated sandstone dissipate significant energy through conversion to the diffusive slow mode. The corresponding peak frequency is

$$f_m \approx \frac{\bar{\kappa} K_f}{\phi\eta a^2}, \tag{29}$$

where here a is the size of the patches and K_f is fluid bulk modulus. Note the inverse dependence on $\bar{\kappa}/\eta$ compared to the Biot mechanism in Eq. (27). Generalization of the Biot theory to the case of multiple material phases and/or double porosity describe more realistic situations (Ba et al. 2015).

8.3 Ductility and Partial Melting. Grain Boundary Relaxation

Seismic propagation in the upper part of the Earth's crust, where geothermal reservoirs are located, shows strong velocity dispersion and attenuation due to different permeability and saturation conditions and is influenced by the brittle–ductile transition (BDT), including zones of partial melting. Under the elastic–plastic aspect, the seismic properties (velocity, quality factor and density) depend on the effective pressure and temperature. The associated effects can be described using the Burgers mechanical model applied to the shear modulus of the dry rock (Carcione, Section 2.4.4). The Arrhenius equation in combination with the octahedral stress criterion defines the Burgers viscosity, which is responsible for the ductile behaviour of partial melting through a process called grain boundary relaxation (Carcione et al. 2018; Carcione 2022, Section 7.23). The viscosity of the earth influences the S-waves so strongly that they disappear when the earth melts completely. P-waves show strong attenuation and scattering (Zener-like peaks) with frequency and temperature—at a critical temperature that depends on frequency and Burgers viscosity. The behaviour of the seismic waves in the presence of partial melting can be used to identify the BDT.

8.4 Thermo-Poroelasticity

Thermoelasticity couples the fields of deformation and temperature. An elastic source leads to a temperature field and wave attenuation, while a heat source causes anelastic deformations. The theory is important in seismology, low-temperature physics, the theory of shocks and vibrations, astrophysics and in the field of nanotechnology. The theory of thermo-poroelasticity predicts a P-wave, an S-wave, a slow Biot wave and a thermal wave with similar properties to the Biot wave (Carcione 2022, Section 7.28; Gurevich and Carcione 2022, Section 2.11). Attenuation in the seismic band can be significant due to the conversion of P-waves to thermal modes in heterogeneous media, which can be referred to as wave-induced thermo-poroelastic attenuation, analogous to wave-induced fluid flow (mesoscopic) damping in connection with the slow Biot mode. The attenuation (dissipation factor or inverse Q) has the form of relaxation peaks (Carcione et al. 2020).

8.5 Example

Consider the material properties for a water-saturated sandstone (see Table 1). Using the Gassmann equations (Carcione 2022, Eq. 7.34), the P-wave velocity is $v_P = 3366$ m/s, and the bulk density is $\rho = 2167$ kg/m^3. Assuming $a = 10$ cm and $r = 0.0008$, the relaxation frequencies of the different attenuation mechanisms are: $f_s = 6.7$ kHz (scattering), $f_B = 213$ kHz (Biot global flow), $f_{sf} = 815$ Hz (squirt flow, with $\phi_c = 0.0002$, $K_h = 12$ GPa) and $f_m = 75$ Hz (mesoscopic). While scattering has a peak at the sonic frequencies and the Biot loss dominates at high (laboratory) frequencies, the squirt-flow and mesoscopic loss mechanisms are important at seismic frequencies. Replacing water with oil ($\rho_f = 800$ kg/m^3, $K_f = 2$ GPa and $\eta = 100$ cP), the peak frequencies are $f_s = 6.8$ kHz, $f_B = 27$ MHz, $f_{sf} = 8$ Hz and $f_m = 0.7$ Hz.

For example, Fig. 3 shows the dissipation factor as a function of frequency, corresponding to brine and light oil (Carcione and Gurevich 2011), where the squirt-flow and Biot peaks can be seen.

8.6 Constant Q Based on Fractional Derivatives

Attenuation can also be modelled with fractional derivatives (e.g. Picotti and Carcione 2017). An example is the fractional Kelvin–Voigt model, where the time derivative of the strain in the dashpot (the overdot) is replaced by ∂_t^q, where q is the order of the derivative. Then, $\sigma = K\epsilon + \eta\partial_t^q\epsilon$, $0 \le q \le 1$, where K is a stiffness, η is a pseudo-viscosity, which is a stiffness for $q = 0$ and a viscosity for $q = 1$. The limits $q = 0$ and $q = 1$ give Hooke's law and the stress–strain of the Kelvin–Voigt model, respectively. In the frequency domain, $M = K + \eta(\mathrm{i}\omega)^q$. If $K = 0$, we obtain a constant $Q = \cot(\pi q/2)$, as in Kjartansson (1979) (see also Carcione 2022, Section 2.5; Mainardi 2022).

9 Bounds and Averages of Q

For composite media, bounds and average values for Q can be defined on the basis of various models (Carcione 2022, Section 7.21). The bounds apply to any medium in which wave propagation undergoes dissipation and velocity dispersion, e.g. for composite-viscoelastic and poro-viscoelastic materials. To obtain complex stiffness constraints and

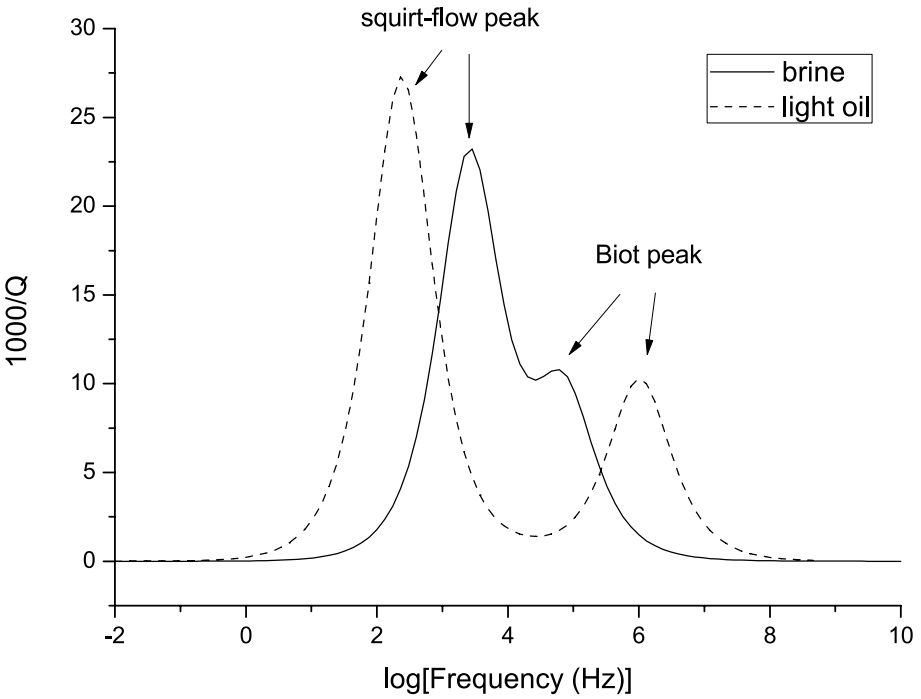

Fig. 3 Dissipation factor as a function of frequency, corresponding to brine and light oil saturating a sandstone

average values, the correspondence principle is applied to calculate the solution of the viscoelastic problem from the corresponding elastic solution. Subsequently, the attenuation is determined for—physical and heuristic—models considering general geometric shapes. The approach is relevant for the seismic characterization of solid composite materials (Carcione 2022, Chapter 8).

10 What Experiments Reveal About *Q*

P-wave dissipation was initially described mainly by phenomenological models represented by mechanical models made of springs and dashpots, such as the standard-linear-solid system, also called the Zener model (Carcione 2022, Section 2.4). However, Zener (1992) obtained this model from thermoelasticity for thin rods as an approximation and the model was already known as a combination of a spring and the Kelvin–Voigt model. An example of the agreement between theory and experiment is shown in Zener (1992, Fig. 8), where a typical relaxation peak ($1/Q$) fitted by the Zener model can be seen.

Knopoff (1964) reports on several experiments. His Fig. 4 shows results obtained by Born in 1941, who examined a sandstone in the laboratory into which different amounts of interstitial water were injected. The dry rock has a Q that does not depend on the frequency; when different amounts of water are injected, the magnitude $1/Q$ increases linearly with the frequency f and α is proportional to f^2. Figure 1 in Knopoff (1964) shows the attenuation

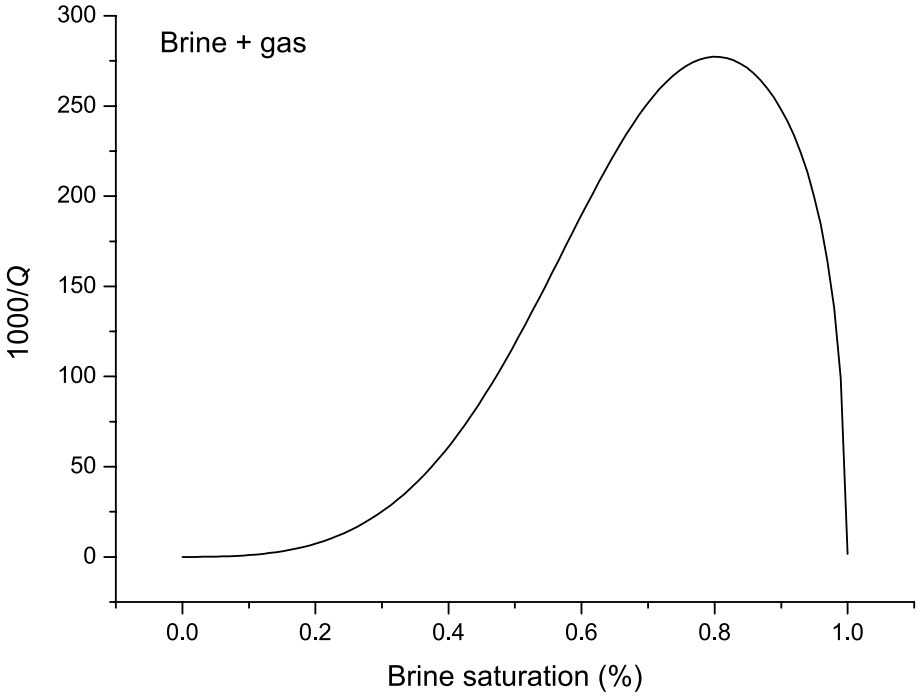

Fig. 4 Dissipation factor as a function of saturation predicted with the White theory

factor as a function of frequency in water, which is found to vary as the square of frequency for different temperatures. Then, Q is inversely proportional to the frequency, as in the previous case. An experiment conducted on the Pierre shale in Colorado, in which pulses were recorded from seismometers placed at various locations in boreholes in the formation, shows an attenuation factor that is linear with frequency in the range of 50–550 Hz (Fig. 11 in McDonal et al. 1958). Consequently, Q is frequency independent in this case.

Murphy (1982) has shown that the extensional-wave loss peaks at 85% water saturation, as can be seen in his Fig. 6. As shown in Fig. 4, this behaviour can be predicted by White's mesoscopic loss theory (right graph), according to which the compressional wave loses energy in gas patches by conversion to slow Biot diffusion modes (Carcione et al. 2006; Carcione 2022, Section 7.16).

Figure 2 in Jones (1986) shows experimental $1000/Q$ (as a broad peak) for extensional waves on a Coconino sandstone from Tittmann and coworkers, who varied the fluid viscosity by mixing water and glycerol and changing the temperature. The data are fitted with a local flow theory from O'Connell (1983). The inputs to this model are the fluid properties and the rock microstructure.

On the other hand, wave attenuation as a function of frequency in the Earth follows power laws, e.g. $Q(\text{P and S}) \propto f^{\nu}$, $0.25 < \nu < 0.6$ and $Q(\text{S}) \propto f^{\nu}$, $1.3 < \nu < 1.7$, as can be seen in Fig. 5 in Ulug and Berckhemer 1984 (mantle) and Fig. 9 in Castro et al. (2008) (crust), respectively.

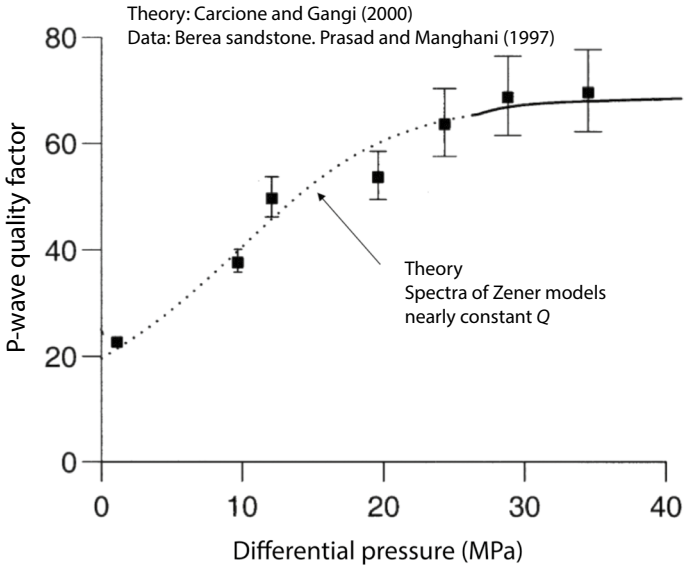

Fig. 5 P-wave quality factor as a function of the differential pressure (confining minus pore)

Carcione and Gangi (2000) report a fit of the ultrasonic (1 MHz) quality factor versus differential (confining minus pore) pressure for water-saturated Berea sandstone (see Fig. 5). The dotted line corresponds to the range 0–2 km, where the rock is normally pressured, and the continuous lines to the range 2–8 km, where the rock is overpressured. The black squares are the experimental bedding-parallel quality factors obtained by Prasad and Manghnani (1997) for Berea sandstone. The quality factor decreases with decreasing differential pressure due to the opening of cracks and the resulting flow effects.

Biot–Gardner effect: When measuring axial or volumetric motions along a porous cylindrical sample (a rod), there is fluid flow at the sides and ends of the sample if these surfaces are not sealed, and open or partially open pore boundary conditions hold. These radial and axial flows induce the Biot–Gardner effect, an "artificial" attenuation peak (and related dispersion) due to the generation of slow (diffusion) Biot modes at the cylinder boundaries, which does not occur for a wave propagating in unbounded media (Carcione 2022, Section 7.17). Therefore, we must distinguish between these effects and the peaks related to intrinsic dissipation in unbounded media. Cheng et al. (2020) show how to remove the Biot–Gardner effect from experimental data to obtain the intrinsic quality factor of the rock.

11 Analogy Between Visco-Elasticity and Electric Circuits

Leonardo Da Vinci was convinced that light has a finite speed. In the Codex Ashburnham (Biblioathèque Nationale, Paris), he declared *It is impossible for the eye to project the visual force from itself by visual rays, since, as soon as it opens, the front [of the eye] which would cause this emanation would have to go out to the object, and this it could not do without time.* Hooke believed that light is a vibrational displacement of the medium through which it propagates at finite speed. Later, in the second half of the 19th century, James Clerk Maxwell and

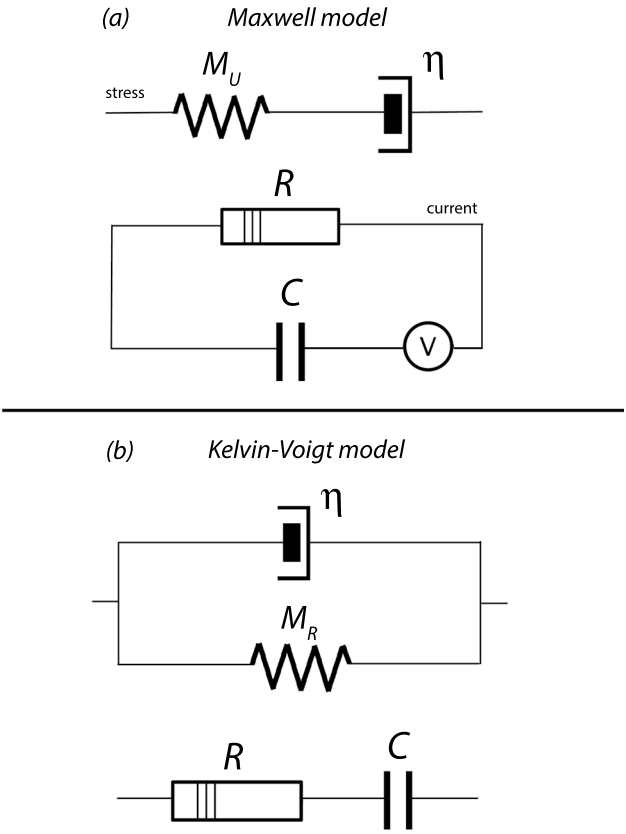

Fig. 6 Examples of analogy between mechanical models and electric circuits

Lord Kelvin used physical and mathematical analogies to investigate wave phenomena in the theory of elasticity, electricity and electromagnetism.

Mathematical analogies are used extensively in many fields of physics (Tonti 1976). The most basic analogy between mechanical models of viscoelasticity and electrical circuits is shown in Fig. 6, where (a) refers to the Maxwell model and (b) to the Kelvin–Voigt model. In these models, a stress is applied to the mechanical model and a current is applied to the electrical circuit.

It can be shown that the quality factor of the Maxwell model is

$$Q = \frac{\omega\eta}{M_U} \tag{30}$$

(Carcione 2022, Eq. 2.176), where η and M_U are the viscosity and stiffness modulus (unrelaxed or high frequency), respectively. For the parallel circuit, we have

$$Q = \omega RC = \frac{\omega\bar{\epsilon}}{\bar{\sigma}} \tag{31}$$

(Carcione 2022, Eq. 8.36), where C and R are the capacitance and resistor, respectively, and $\bar{\epsilon}$ (C) and $\bar{\sigma}$ ($1/R$) are the associated dielectric constant and electrical conductivity,

respectively. It is clear the mathematical analogy: $\eta \to R$ and $M_U \to C^{-1}$. If $\eta = 0$, the stored energy is zero, because the absence of the dashpot implies a discontinuity of the stress and $Q = 0$ (all energy is lost).

On the other hand, for the Kelvin–Voigt model and series circuit it is

$$Q = \frac{M_R}{\omega\eta} \tag{32}$$

(Carcione 2022, Eq. 2.184), where M_R is the relaxed (or zero frequency) stiffness modulus, and the analogy implies

$$Q = \frac{1}{\omega RC} = \frac{\bar{\sigma}}{\omega\bar{\epsilon}}. \tag{33}$$

In this case $\eta = 0$, implies that all the energy is stored in the spring and $Q = \infty$.

In a more general situation, an analogy (Carcione 2022, Eq. 8.135) can be made between the standard-linear-solid (Zener) model (Carcione 2022, Section 2.4.3) and the Debye circuit consisting of two capacitors and a resistor (Carcione 2022, Fig. 8.3).

12 A Practical Application

We consider the data in Figs. 2 and 4 of Cadoret et al. (1995) (velocity versus water saturation) and Fig. 1 in Cadoret et al. (1998) (Q factor versus water saturation, $1000/Q_E$ closed). The rock is Estaillades limestone, the frequency is 1 KHz (sonic band), the porosity is 0.3, the permeability is 255 mdarcy and the experiment is a drying one, where gas (CO_2) patches are created. The experiment is performed at atmospheric pressure in resonant bars. The data are given as extensional-wave velocity, v_E, shear-wave velocity, v_S, and extensional-wave quality factor, Q_E. To obtain the P-wave values (v_P and Q_P), we use Eqs. (19) and (20), and Cadoret et al. (1995)

$$v_P^2 = \frac{v_S^2(4v_S^2 - v_E^2)}{3v_S^2 - v_E^2} \tag{34}$$

(to be used for Poisson ratios, $\nu < 0.4$; here the range is 0.22–0.29), where (Mavko et al. 2020)

$$\nu = \frac{(v_P/v_S)^2 - 2}{2[(v_P/v_S)^2 - 1]} \tag{35}$$

and we assume $Q_S = 270$ at all saturations (see Fig. 3 in Cadoret et al. 1998)). In the case of shear waves, the test results show a slight variation in velocity with frequency. The variation of shear-wave velocity with saturation in Cadoret et al. (1995) is explained by the density effect, so that there is practically no velocity dispersion and the attenuation is very weak. Table 1 in Pang et al. (2019) contains the values of the different properties, and the data are shown in Fig. 7. The saturations correspond to the experimental points of the axial or extensional velocities v_E. The quality factors Q_E were linearly interpolated to these points. Figure 8 shows the dissipation factor versus the P-wave velocity used in the rock physics template (see below).

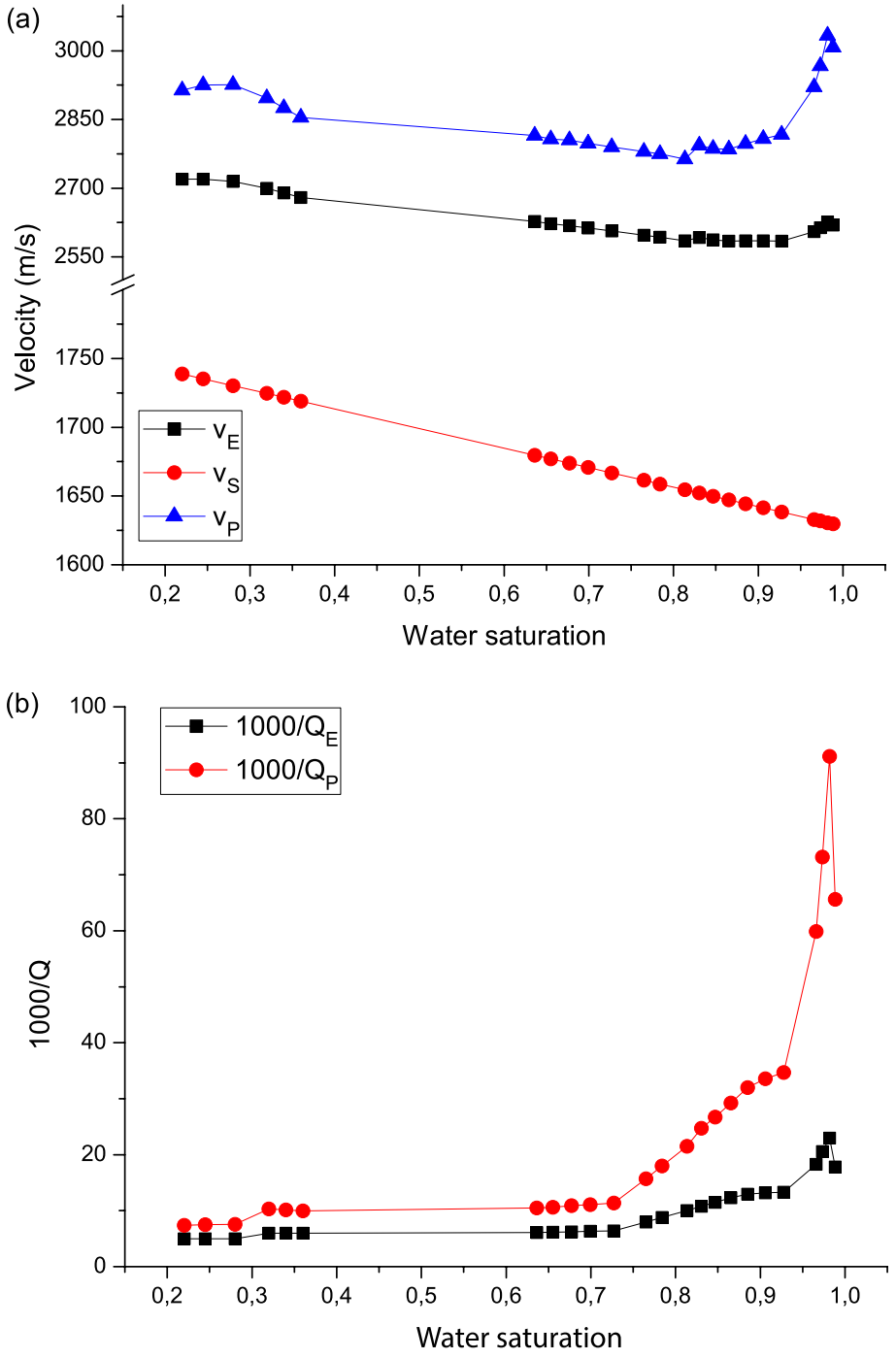

Fig. 7 Velocities (**a**) and dissipation factors (**b**) versus water saturation in Estaillades limestone

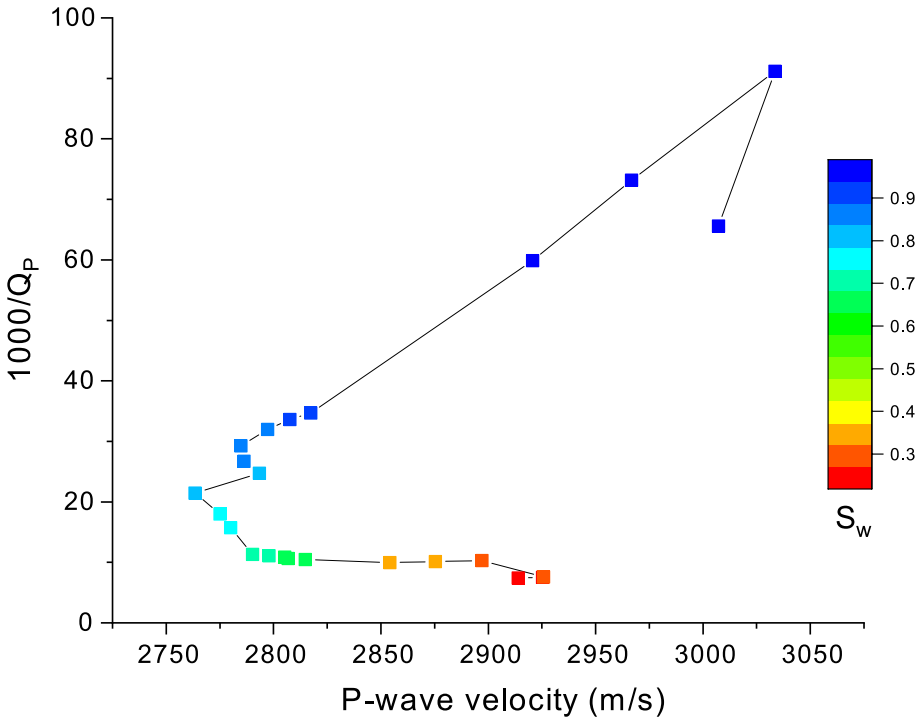

Fig. 8 Dissipation factor versus P-wave velocity and varying brine saturation

Table 1 in Pang et al. (2019) shows the properties for fitting the data with the Biot-White model (Carcione 2022, Section 7.16). Supplementary microstructural data on the Estaillades limestone can be found in (Rasolofosaon and Zinszner, Fig. 2). We use Krief model to obtain the dry rock bulk and shear moduli

$$\begin{aligned} K_m &= K_s(1-\phi)^{A/(1-\phi)}, \qquad \text{and} \\ \mu_m &= K_m \mu_s / K_s, \end{aligned} \tag{36}$$

, respectively, where A is a constant and μ_s is the shear modulus of the grains. Permeability is related to porosity by the Kozeny–Carman relation

$$\kappa = \frac{\kappa_0 \phi^3}{(1-\phi)^2} \tag{37}$$

where κ_0 is a constant (Pang et al. 2019). Figure 9 compares the theoretical and experimental results. The radius of the gas patches is 5 mm. The template is shown in Fig. 10 and, as can be seen, enables the determination of porosity and saturation when the experimental data (symbols, obtained from inversion techniques) are superimposed to the template.

Estimating the seismic Q is more difficult than in the laboratory due to many factors. Due to the low-frequency content of seismic waves, attenuation effects are usually small and can generally only be measured with accuracy over long distances. In addition, amplitudes can be affected by other factors, such as reflection/transmission phenomena

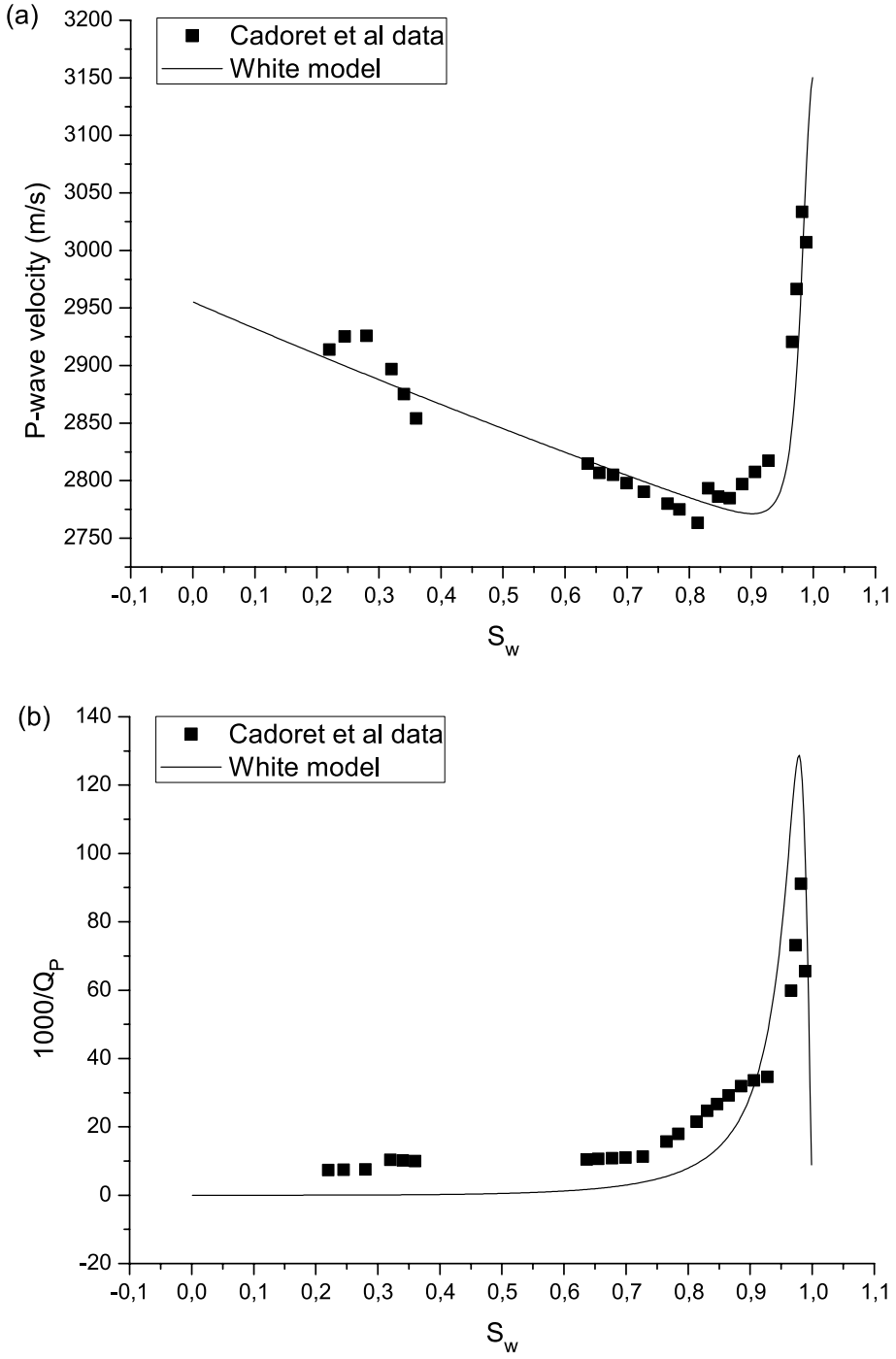

Fig. 9 P-wave velocity (**a**) and dissipation factor (**b**) versus water saturation. Fit with White mesoscopic model (solid line). The radius of the gas patches is 5 mm

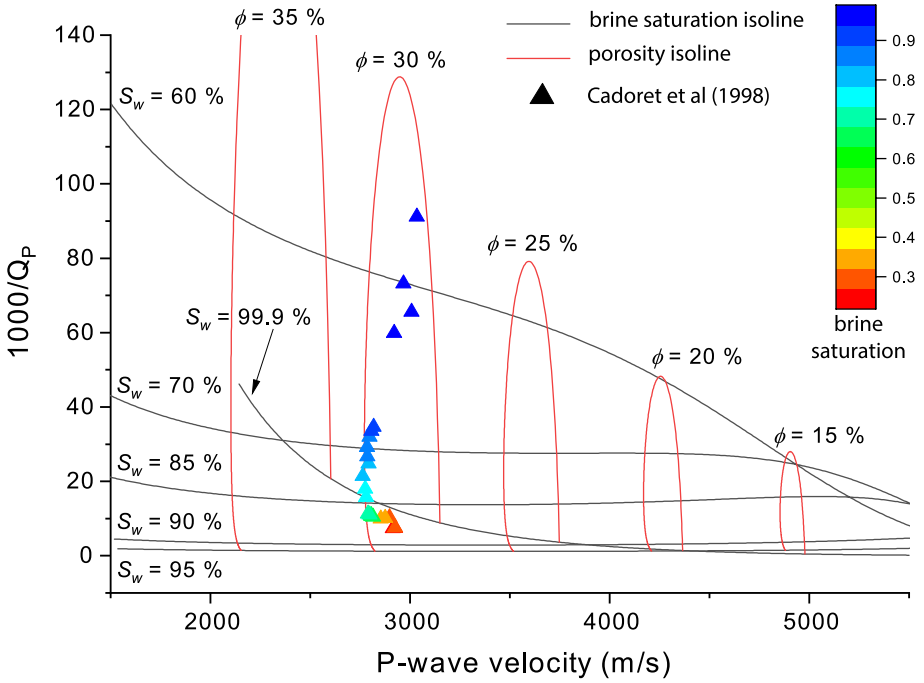

Fig. 10 Rock physics template of dissipation factor versus P-wave velocity, with isolines of porosity and brine saturation

Table 1 Sandstone properties

Grain	Bulk modulus, K_s	40	GPa
	Density, ρ_s	2650	kg/m^3
Matrix	Porosity, ϕ	0.3	
	Bulk modulus, K_m	10	GPa
	Shear modulus, μ_m	8	GPa
	Permeability, $\bar{\kappa}$	100	mD
	Tortuosity, $\mathcal{T}$	2.3	
Fluid	Bulk modulus, K_f	2.25	GPa
	Density, ρ_f	1040	kg/m^3
	Viscosity, η	1	cP

and low signal-to-noise ratios. Picotti and Carcione (2006) have successfully tested the reliability of the spectral ratio and frequency shift methods for estimating the intrinsic quality factor in the presence of random noise. Rossi et al. (2007) estimate the quality factor from seismic reflections using a tomographic inversion algorithm based on the frequency shift method. The combined use of travel time and attenuation tomography provides a 3D velocity–Q cube that was used to map the spatial distribution of gas-hydrate concentration and free gas saturation. Pang et al. (2021) estimate seismic Q and relate it to fluid saturation based on the self-consistent approximation and poroelasticity

theory to create a rock physics template and evaluate gas reserves in tight sandstones. A similar technique is applied to carbonates by Pang et al. (2019).

13 Conclusions

We have shown that the quality factor Q used in the seismic-elastic literature can be different due to several factors: the shape of the medium, the spatial dimension, the use of the strain energy or the total energy, the type of wave (propagating or stationary), the type of loss mechanism (in poroelasticity) and the inhomogeneity of the wave. We also consider the analogy between elastic and electromagnetic waves and discuss theories based on relaxation peaks, bounds on Q and experiments showing the behaviour of Q as a function of frequency, saturation and pore pressure.

Declarations

Conflict of interest The authors declare that they have no conflict of interest.

References

Ba J, Carcione JM, Du O, Zhao H, Müller TM (2015) Seismic exploration of hydrocarbons in heterogeneous reservoirs: New theories, methods applications. Elsevier Science, NJ, p 10

Borcherdt RD (2009) Viscoelastic waves in layered media. Cambridge University Press, Cambridge, p 12

Buchen PW (1971) Plane waves in linear viscoelastic media. Geophys J R Astron Soc 23:531–542

Cadoret T, Marion D, Zinszner B (1995) Influence of frequency and fluid distribution on elastic wave velocities in partially saturated limestones. J Geophys Res 100(B6):9789–9803

Cadoret T, Mavko G, Zinszner B (1998) Fluid distribution effect on sonic attenuation in partially saturated limestones. Geophysics 63:154–160

Castro RR, Gallipoli MR, Mucciarelli M (2008) Crustal Q in southern Italy determined from regional earthquakes. Tectonophysics 457(2):96–101

Carcione JM (2001) Energy balance and fundamental relations in dynamic anisotropic poro-viscoelasticity. Proc Roy Soc London Ser A 457:331–348

Carcione JM (2022) Wave fields in real media. Theory and numerical simulation of wave propagation in anisotropic, anelastic, porous and electromagnetic media, 4th edn. Elsevier, New Jersey, p 10

Carcione JM, Ba J (2024) Test of the relation between temporal and spatial Q by Knopoff et al. submitted to Wave Motion

Carcione JM, Cavallini F (1993) Energy balance and fundamental relations in anisotropic-viscoelastic media. Wave Motion 18:11–20

Carcione JM, Cavallini F (1994) A rheological model for anelastic anisotropic media with applications to seismic wave propagation. Geophys J Int 119:338–348

Carcione JM, Gangi A (2000) Non-equilibrium compaction and abnormal pore-fluid pressures: effects on seismic attributes. Geophys Prosp 48:521–537

Carcione JM, Gei D, Santos JE, Fu L-Y, Ba J (2020) Canonical analytical solutions of wave-induced thermoelastic attenuation. Geophys J Int 221:835–842

Carcione JM, Gurevich B (2011) Differential form and numerical implementation of Biot's poroelasticity equations with squirt dissipation. Geophysics 76:N55–N64

Carcione JM, Picotti S, Gei D, Rossi G (2006) Physics and seismic modeling for monitoring CO2 storage. Pure Appl Geophys 163:175–207

Carcione JM, Poletto F (2000) Simulation of stress waves in attenuating drill strings, including piezoelectric sources and sensors. J Acoust Soc Am 108(1):53–64

Carcione JM, Liu X, Greenhalgh S, Botelho MAB, Ba J (2020) Quality factor of inhomogeneous plane waves. Phys Acoust 66:598–603

Carcione JM, Poletto F, Farina B, Bellezza C (2018) 3D seismic modeling in geothermal reservoirs with a distribution of steam patch sizes, permeabilities and saturations, including ductility of the rock frame. Phys Earth Planet Inter 279:67–78
Carcione JM, Zhu T, Picotti S, Gei D (2016) Imaging septaria with *Q* compensation by reverse-time migration. Netherlands J Geosci. https://doi.org/10.1017/njg.2016.2
Cheng W, Carcione JM, Qadrouh A, Alajmi M, Ba J (2020) Rock anelasticity, pore geometry and the Biot-Gardner effect, Rock Mech. Rock Eng 53:3969–3981
Frankel A, Wennerberg L (1987) Energy-flux model of seismic coda: separation of scattering and intrinsic attenuation. Bull Seism Soc Am 77(4):1223–1251
Green EI (1955) The story of *Q*. Am Sci 43:584–594
Gurevich B, Carcione JM (2022) Attenuation and dispersion in fluid-saturated porous rocks: Mechanisms and models. Soc Explorat Geophys 26:9781560803911
Jones TD (1986) Pore-fluids and frequency dependent-wave propagation rocks. Geophysics 51:1939–1953
Kikuchi M (1981) Dispersion and attenuation of elastic waves due to multiple scattering from cracks. Phys Earth Planet Inter 27:10–105
Kjartansson E (1979) Constant Q wave propagation and attenuation. J Geophys Res 84:4737–4748
Knopoff L (1964) *Q* reviews. Geophysics 2(4):625–660
Knopoff L, Aki K, Archambeau CB, Ben-Menahem A, Hudson JA (1964) Attenuation of dispersed waves. J Geophys Res 64(8):1655–1657
McDonal FJ, Angona FA, Milss RL, Sengbush RL, van Nostrand RG, White JE (1958) Attenuation of shear and compressional waves in Pierre shale. Geophysics 23:421–439
Mainardi F (2022) Fractional calculus and waves in linear viscoelasticity. World Scientific
Mavko G, Mukerji T, Dvorkin J (2020) The rock physics handbook. Cambridge Univ, Press
Müller TM, Gurevich B, Lebedev M (2010) Seismic wave attenuation and dispersion resulting from wave-induced flow in porous rocks - a review. Geophysics 75(5):A147–A164
Murphy WF III (1982) Effects of partial water saturation on attenuation Massilon sandstone and Vycor porous glass. J Acous Soc Am 71(6):1458–1468
O'Connell RJ (1983) A viscoelastic model of anelasticity of fluid saturated porous rocks. In: Johnson, D. L., and Sen, P. N., Eds., Am. Inst. Phys., Proceedings, Am. Inst. Phys. conference on physics and chemistry of porous media, Schlumberger-Doll Research, pp 166176
Pang M, Ba J, Carcione JM (2021) Characterization of gas saturation in tight-sandstone reservoirs with rock-physics templates based on Seismic *Q*. J Energy Eng 147(3):04021011
Pang M, Ba J, Carcione JM, Picotti S, Zhou J, Jiang T (2019) Estimation of porosity and fluid saturation in carbonates from rock-physics templates based on seismic *Q*. Geophysics 84:M25–M36
Picotti S, Carcione JM (2006) Estimating seismic attenuation (Q) in the presence of random noise. J Seismic Explor 15:165–181
Picotti S, Carcione JM (2017) Numerical simulation of wave-induced fluid flow seismic attenuation based on the Cole-Cole model. J Acoust Soc Am 142(1):134–145
Prasad M, Manghnani MH (1997) Effects of pore and differential pressure on compressional wave velocity and quality factor in Berea and Michigan sandstones. Geophysics 62:1163–1176
Qadrouh AN, Carcione JM, Alajmi M, Ba J (2024) Seismic *Q* revisited, submitted.
Rasolofosaon PN, Zinszner BE (2007) The unreasonable success of Gassmann's theory Revisited. J Seismic Explor 16:281–301
Rossi G, Gei D, Böhm G, Madrussani G, Carcione JM (2007) Attenuation tomography: An application to gas-hydrate and free-gas detection. Geophys Prosp 55:655–669
Spencer JW (1981) Stress relaxations at low frequencies in fluid-saturated rocks: attenuation and modulus dispersion. J Geophys Res 86(B3):1803–1812
Tonti E (1976) The reason for analogies between physical theories. Appl Math Model 1:37–50
Ulug A, Berckhemer G (1984) Frequency dependence of *Q* for seismic body waves in the Earth's mantle. J Geophys 56:9–19
White JE (1975) Computed seismic speeds and attenuation in rocks with partial gas saturation. Geophysics 40:224–232
Zener C (1992) 1946. American institute of mining and metallurgical engineers, Technical Publication No, Anelasticity of metals